Upper Limit Branching Ratios for Decays Involving K_s

University of Colorado REU report

R.S. uc er

August 9, 2006

1 Introduction

1.1 Research Experience for Undergraduates Overview

This summer I worked with Profs. John Cumalat and Kevin Stenson in high energy physics. My project was to look at data from FOCUS (a.k.a. E831 at Fermilab) to determine if the rare decays $D^0 \to K_s\pi^+\pi^-\pi^+\pi^-\pi^+$, $D^+ \to K_s\pi^+\pi^-\pi^+\pi^-\pi^+\pi^-$, $D^+ \to K_sK_sK_s\pi^+$, and $D_s^+ \to K_s\pi^+$ could be observed. I then compared these decays to other, previously seen decays to set upper limit branching ratios.

1.2 FOCUS

The FOCUS experiment (aka E831) is a charm photoproduction experiment. It is located in the Wideband Area of Fermilab and collected data during the 1996-1997 fixed target run. Reconstruction of data began in 1998 and was finished by the end of 1999. The analysis of this data continues to the present.

1.2.1 FOCUS Beamline

The FOCUS beamline begins as a proton beam, accelerated from rest to 800 GeV using a series of five accelerators. It begins as hydrogen gas, ionized by the addition of electrons. The H^- ions are accelerated electrostatically to .750 MeV through a system of voltage dividing nodes (Cockcroft-Walton). They are then accelerated to 400 MeV using a linear accelerator (LINAC). LINAC is a series of alternating high field and free field regions. As the ions exit LINAC, they pass through a thick carbon foil which strips the ions of their electrons, leaving only protons. The booster, a synchotron about 500 ft. in diameter, accelerates a group of protons to 8 GeV. It takes 12 groups of protons to fill the main ring at Fermilab. The main ring accelerates the protons to 150 GeV and injects them into the Tevatron. The Tevatron uses liquid helium cooled superconduction dipole magnets to contain the proton beam and accelerate it to 800 GeV. The main ring and the Tevatron are both synchotrons with diameter 1 km.

Proton extraction is a process of slowly removing the beam and sending it down fixed target beamlines. Electrostatic devices and magnets in the switchyard split and direct the beam into three major areas: proton, neutrino, and meson. The beams in each of these areas are again split. The radio frequency acceleration cavities of the Tevatron operate at 53 MHz, which means that the protons arrive at the experiment in regularly spaced 18 ns intervals.

To create the photon beamline, incident 800 GeV protons strike a cryogenically cooled liquid deterium target. The interactions produce many particles, but specifically they produce π^0s that decay into 2 photons. A series of magnets and converters remove the other particles produced in the interactions. Powerful diple magnets sweep away charged particles. The neutral particles in the beam strike a photon converter, which is a piece of lead 50% of a radiation thick. In this process, the photons convert to e^+e^- pairs and other particles pass through. Quadropole magnets focus the electrons and positrons. These magnets bend the charged portion of the beam around a dump that collects non-interacting neutral particles. Momentum recombining dipoles recombine the electrons and positrons (which have been split into two beams). The recombined beam is then focused and strikes the

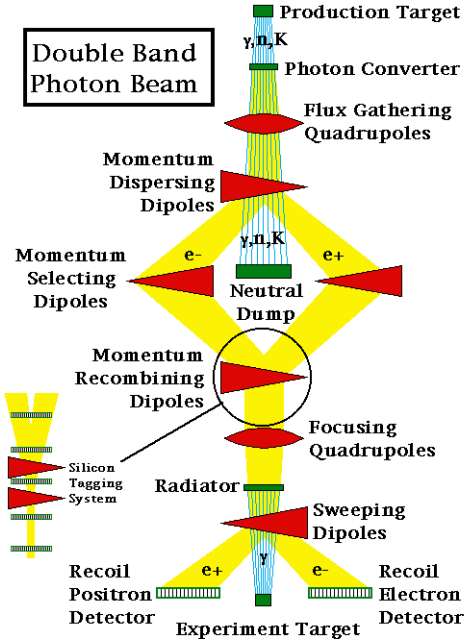

Figure 1: FOCUS Beamline

radiator, a sheet of lead 20% of a radiation thick, where the bremsstralung process produces photons. Sweeping dipoles redirect the charged portion of the beam to a recoil positron detector and a recoil electron detector. The neutral part of the beam continues towards the experiment target. The mean energy of the photons is around 190 GeV. A lead wall and lead collimator remove background synchotron radiation.

An advantage to this process is that the interactions in the primary target caused by hadrons in the beam are greatly reduced, as the hadron contamination of the beam is very low. A disadvantage to this process is that very few photons are generated relative to the number of protons in the beam.

1.2.2 FOCUS detector

The FOCUS detector is actually a system of smaller devices and detectors. These detectors provide particle tracking and identification.

The following devices track and vertex particles in the FOCUS detector. Silicon microstrips are essentially reverse bias semiconductors. Charge produced by ionizing particles is gathered at the end of each strip. A multiwire proportional chamber (PWC) is a mesh of wires in several planes. Each plane is alternately high voltage or grounded. The PWC is placed in a gas chamber, so that charged particles passing through ionize gas molecules. The electric field accelerates the electrons removed from these particles toward the grounded wires. Along the way, the electrons ionize more of the gas, and the cascade of charge that develops is deposited on the grounded wires. Straw tube chambers use the same concepts as PWCs. The difference between the two is that the voltage in a straw tube chamber is across a metal tube with a ground wire running through the center. In between these tracking devices are two magnets. The change in the slopes of the tracks through the magnets is used to find the momentum of a particle.

The following devices help with particle identification. Cerenkov detectors rely on the Cerenkov effect to tell the difference between pions, kaons, and protons. The Cerenkov effect is a “shockwave” of light produced when a particle travels faster than light travels through a specific medium. The presence or absence of this light is an indication of the particle identification. Calorimeters destructively measure the energy of particles. In electromag-

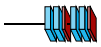

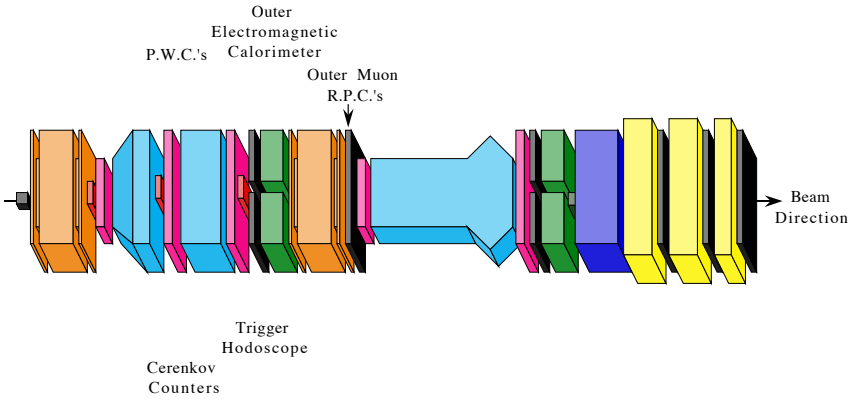
Outer
Electromagnetic
Calorimeter
P.W.C.'s
Outer Muon
R.P.C.'s
Beam
Direction
Trigger
Hodoscope
Cerenkov
Counters

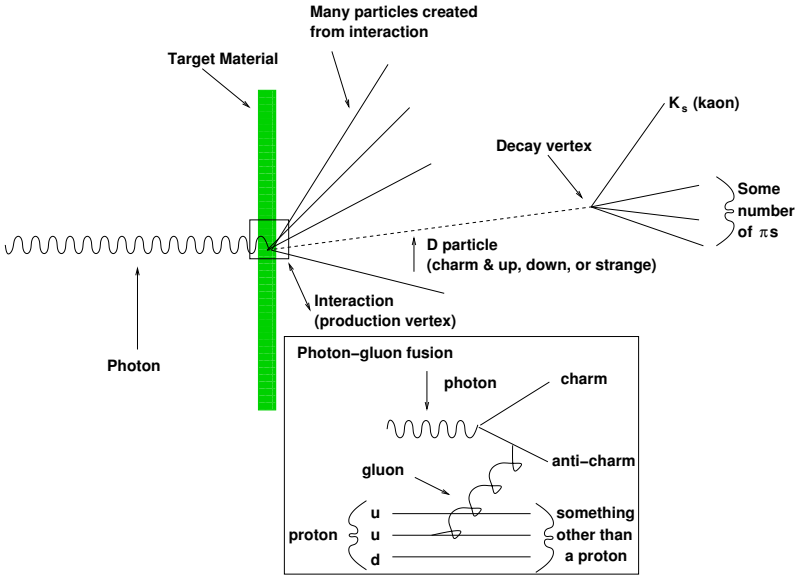

Figure 3: Creation of D particles and subsequent decay

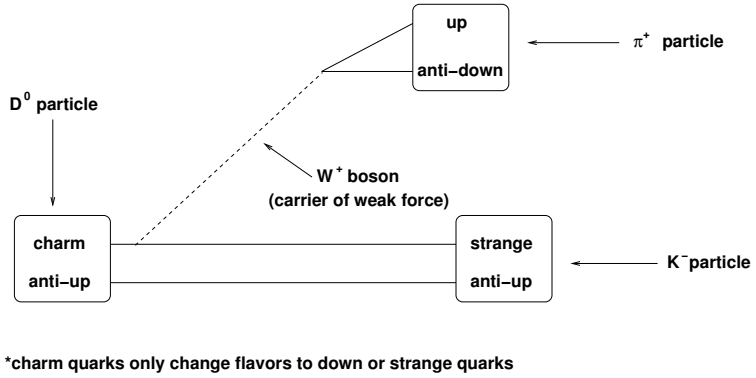

Figure 4: An example of a D^0 particle decaying to a kaon and a pion

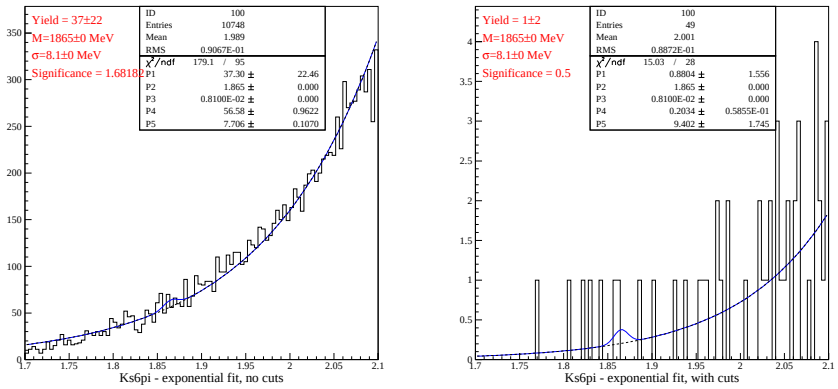

Figure 5: $K_s6\pi$ data- single Gaussian with exponential background, before and after cuts are applied

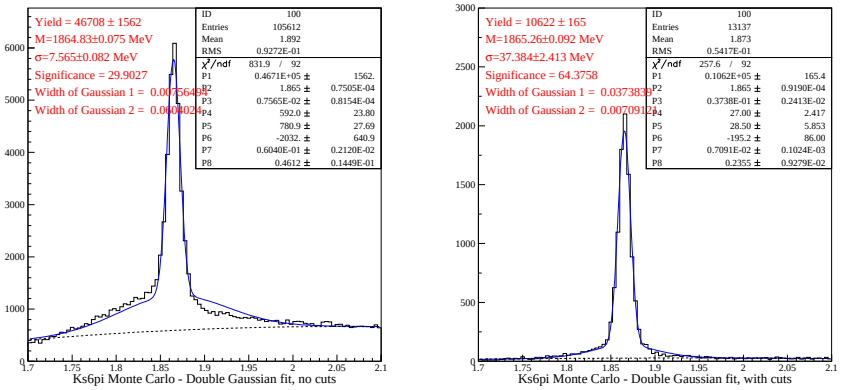

Figure 6: $K_s6\pi$ Monte Carlo - double Gaussian with quadratic background, before and after cuts are applied

2 Applied Cuts

Each of the four channels I worked with this summer required similar techniques. In each ntuple of data, the signal (if it exists) is obscured by tremendous amounts of background. We try to isolate the signal by reducing background. We do this by cutting events based on certain kinematic variables. Additionally, Monte Carlo methods are used to simulate the data. The Monte Carlo is used as a measure of efficiency in the branching ratio. This section includes plots of both data and Monte Carlo for every signal and normalization channel. In each figure, the plot on the left is a mass plot with no cuts applied and the plot on the right is a mass plot with the final cuts applied. Mass (measured in GeV) is on the x-axis and the number of events is on the y-axis.

2.1 $K_s\pi^+\pi^-\pi^+\pi^-\pi^+\pi^-/K_s\pi^+\pi^-\pi^+\pi^-$

There was no easily observable signal in the $K_s6\pi$ data, so the cuts were chosen by maximizing the Monte Carlo signal divided by the square root of the data background. The normalization mode for $K_s6\pi$ is $K_s4\pi$. For this channel, we required that the distance between the primary vertex and the secondary vertex, divided by the error in that distance be greater than 8. For the pion daughters, we required that non-pion hypotheses be favored over the pion hypothesis by no more than 5 units of log-liklihood. We required that there be more than two tracks in

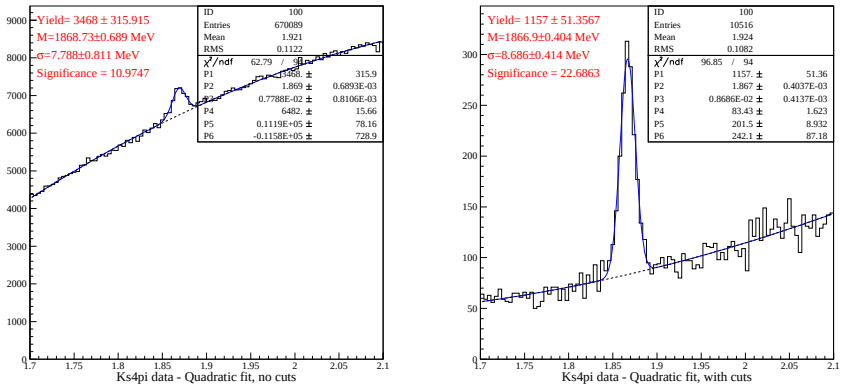

Figure 7: $K_s 4\pi$ data - single Gaussian with quadratic background, before and after cuts are applied

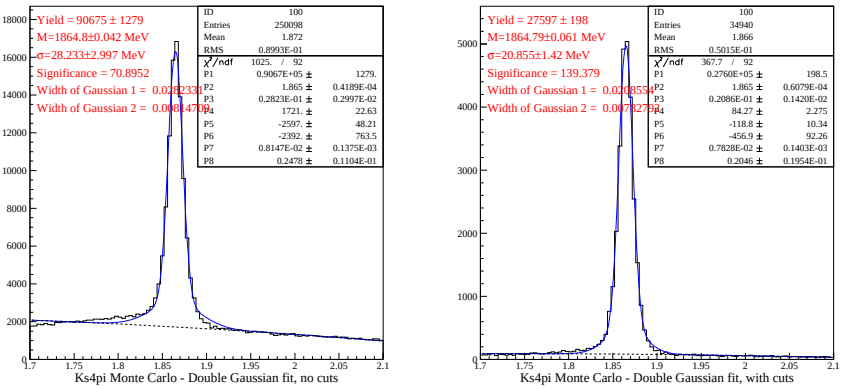

Figure 8: $K_s 4\pi$ Monte Carlo- double Gaussian with quadratic background, before and after cuts are applied

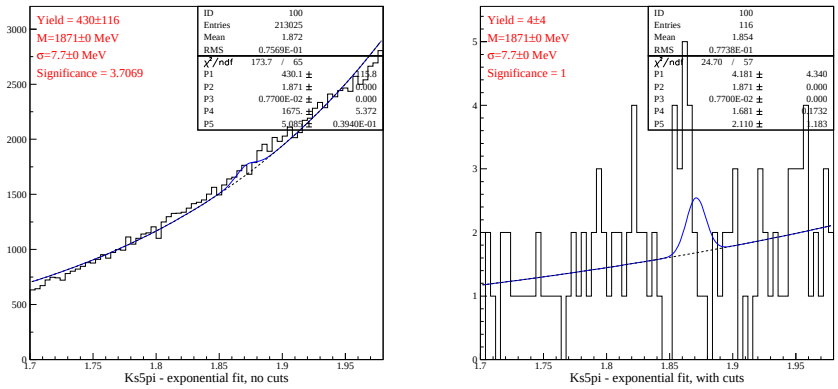

Figure 9: $K_s5\pi$ data- single Gaussian with exponential background, before and after cuts are applied

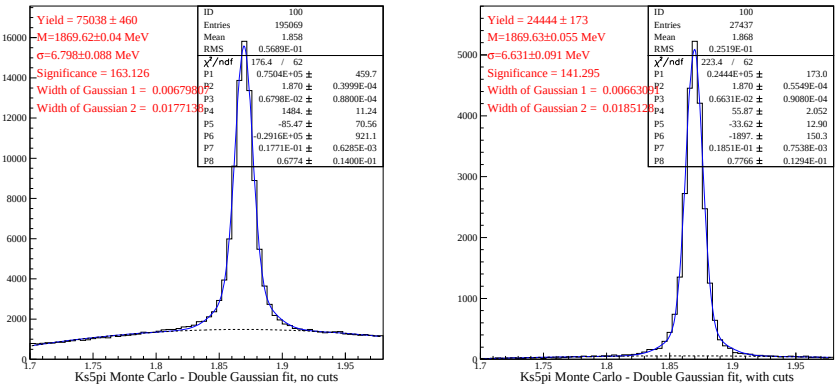

Figure 10: $K_s5\pi$ Monte Carlo - double Gaussian with quadratic background, before and after cuts are applied

the primary vertex. We required that there be only one candidate per event. The justification for this cut is that we choose only one candidate per event because it is highly unlikely that more than two charm particles are created in each event. Even so, we usually only see one or two charm particles. We choose only the best candidate, based on whether it comes from a D^*, has more than two tracks in the primary vertex, and has the highest l/sig (length between primary and secondary vertices divided by the error in that length). We eliminate any tracks consistent with being e^+e^- pairs. We require that the error in the proper lifetime of the D^0 particle be less than 0.08. Lastly, we require that adding tracks from the secondary vertex into the primary vertex does not significantly increase the confidence level of the primary vertex.

2.2 $K_s\pi^+\pi^-\pi^+\pi^-\pi^+/K_s\pi^+\pi^-\pi^+$

There was no easily observable signal in the $K_s5\pi$ data, so the cuts were chosen by maximizing the Monte Carlo signal divided by the square root of the data background. The normalization mode for $K_s5\pi$ is $K_s3\pi$. For this channel, we required that the distance between the primary vertex and the secondary vertex, divided by the error in that distance be greater than 15. For the pion daughters, we required that non-pion hypotheses be favored over the pion hypothesis by no more than 5 units of log-liklihood, that is, the pi consistency had to be larger than -5.0. We required that there be more than two tracks in the primary vertex. We required that there be only one

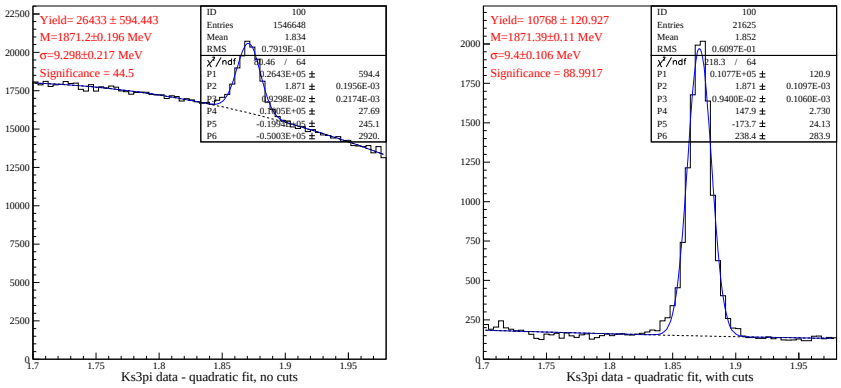

Figure 11: $K_s3\pi$ data - single Gaussian with quadratic background, before and after cuts are applied

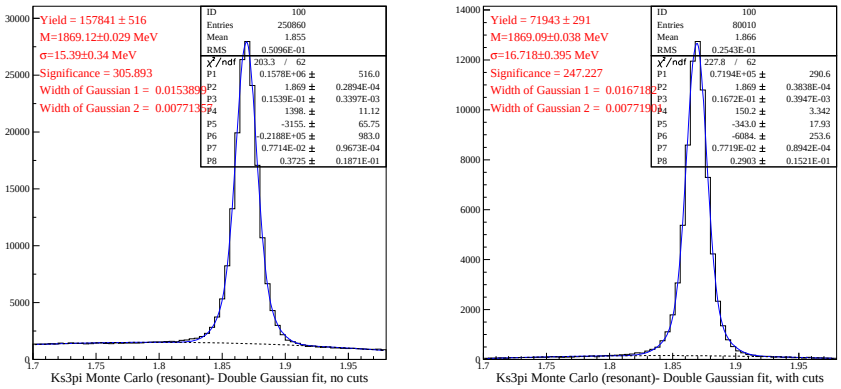

Figure 12: $K_s3\pi$ Monte Carlo- double Gaussian with quadratic background, before and after cuts are applied

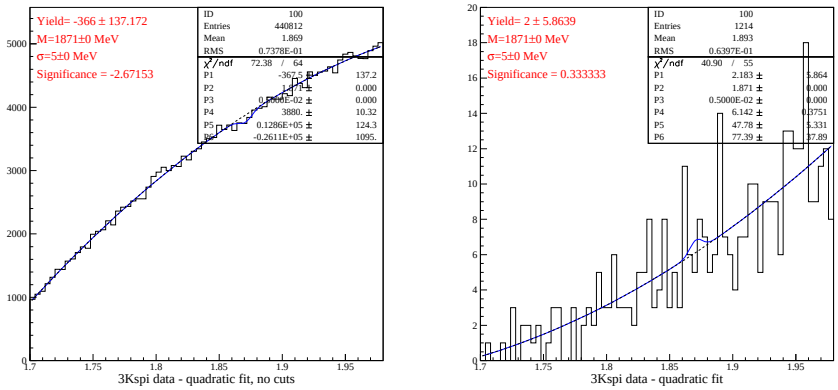

Figure 13: $3K_s\pi$ data- single Gaussian with quadratic background, before and after cuts are applied

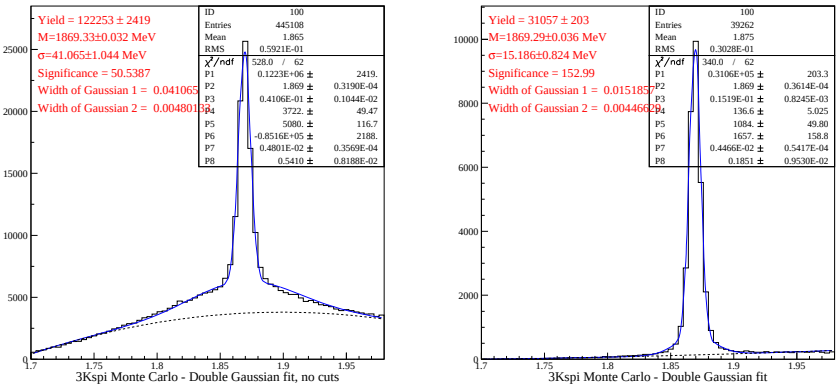

Figure 14: $3K_s\pi$ Monte Carlo - double Gaussian with quadratic background, before and after cuts are applied

candidate per event. The justification for this cut is the same as above. We eliminate any tracks consistent with being e^+e^- pairs. We require that the momentum of the D^0 particle be greater than 40 GeV. We require that the D^0 particle decays outside the the material. Lastly, we require that adding tracks from the secondary vertex into the primary vertex does not significantly increase the confidence level of the primary vertex.

2.3 $K_sK_sK_s\pi^+/K_s\pi^+\pi^-\pi^+$

There was no easily observable signal in the $3K_s\pi$ data, so the cuts were chosen by maximizing the Monte Carlo signal divided by the square root of the data background. The normalization mode for $3K_s\pi$ is $K_s3\pi$. For this channel, we required that the distance between the primary vertex and the secondary vertex, divided by the error in that distance be greater than 3. For the pion daughters, we required that non-pion hypotheses be favored over the pion hypothesis by no more than 5 units of log-liklihood. We eliminate any tracks consistent with being e^+e^- pairs. We require that the momentum of the D^0 particle be greater than 40 GeV. We do not allow different vees to share the same tracks. We require that the maximum absolute value of the normalized mass of any of the kaon daughters be less than three standard deviations of the nominal K_s mass. Lastly, we require that difference between the D^0 mass and the combined $3K_s$ mass be greater than 0.15.

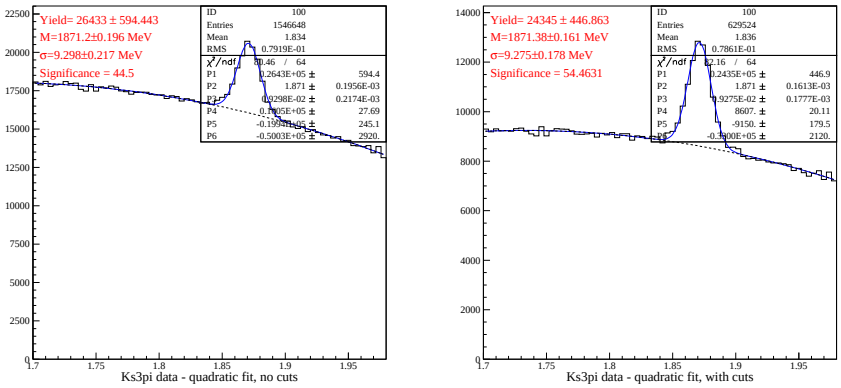

Figure 15: $K_s3\pi$ data - single Gaussian with quadratic background, before and after cuts are applied

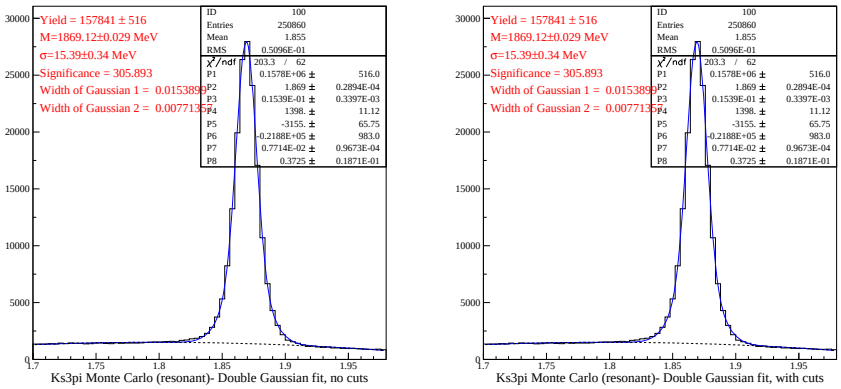

Figure 16: $K_s3\pi$ Monte Carlo- double Gaussian with quadratic background, before and after cuts are applied

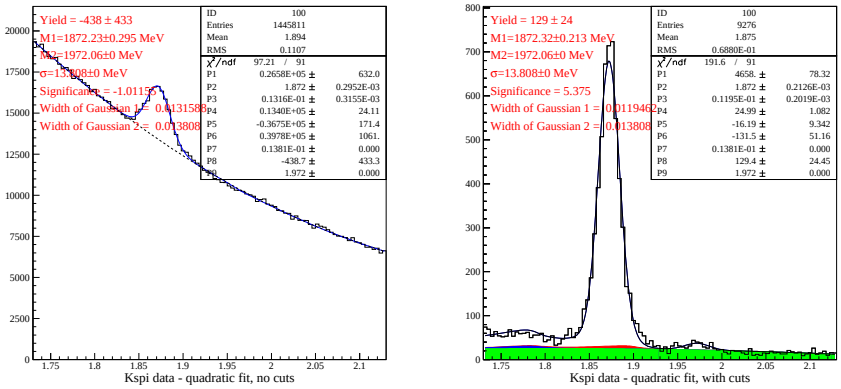

Figure 17: $K_s\pi$ data- single Gaussians with quadratic background, before and after cuts are applied

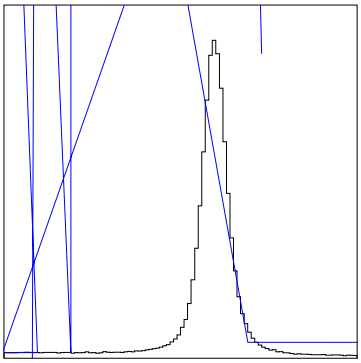

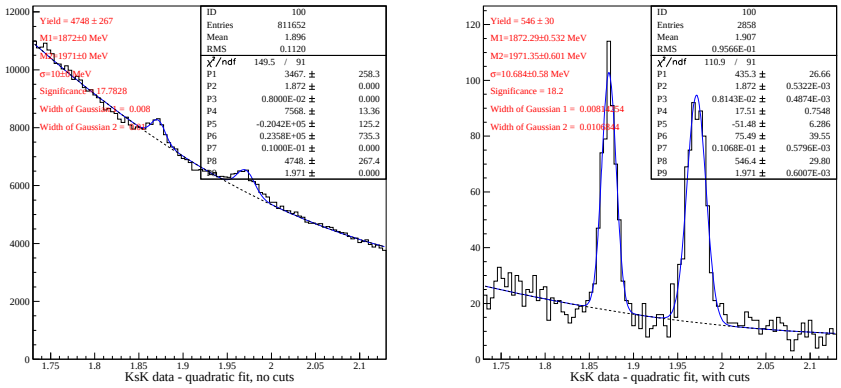

Figure 19: K_sK data- single Gaussians with quadratic background, before and after cuts are applied

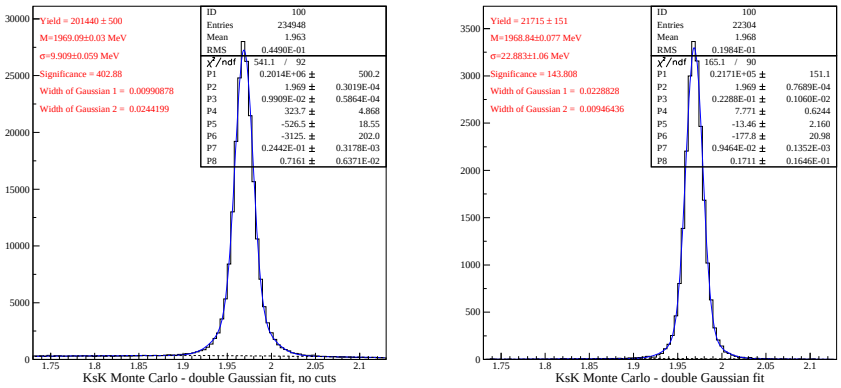

Figure 20: K_sK Monte Carlo- double Gaussian with quadratic background, before and after cuts are applied

momentum of the D^0 had to be larger than 40 GeV and the momentum of the pion had to be larger than 15 GeV. We eliminated daughters consistent with being electrons. We also required that different vees cannot share tracks. We used an isolation cut on the secondary vertex of less 0.02. We required that the reduced chi-squared (χ^2/DOF) for fit to the track of the daughters be less than 0.2. We also cut on the intersection of the pion and the $K_s\pi$ momentum vector. For vee type 1, we used an l/sig cut greater than 11 and an isolation cut on the secondary vertex less than 0.2. For vee type 4, we used an l/sig greater than 9. For vee type 5, we used an l/sig cut greater than 10.

Vee type 9 is the only non-magnet vee type, and it had a seperate set of cuts. We used an l/sig cut greater than 7. We required that other tracks put into the secondary vertex could not increase the confidence level of the secondary vertex. We required the same for the primary vertex. We required the error on the lifetime of the D^0 be less than .12 ps. Lastly, we required that the error in the z-coordinate of the vertex of the vee be less than 1.5.

3 Fitting the plots

In order to determine the number of events in each signal, we fit the data or Monte Carlo with some type of Gaussian function. For the high multiplicity channels ($K_s6\pi$ and $K_s5\pi$) we use a Gaussian function with an exponential background to fit the data. Because there is no signal, the Gaussian has a fixed mass and width. For the other channel in which we do not see a signal ($3K_s\pi$), we use a Gaussian function with a quadratic background. Again, its mass and width are fixed. For all four channels described in this report, the Monte Carlo plots were fitted with a double Gaussian function with a quadratic background. The $K_s\pi$ data was fitted with a Gaussian function with a quadratic background, as well. The mass and width of the large Gaussian (the D^+ peak) were not fixed, while the mass and width of the smaller Gaussian (the D_s^+ peak) were held fixed. In the instances when we had to fix either the mass or the width, the values for these variables were chosen by using the comparable Monte Carlo values.

Both the $K_s\pi$ and K_sK plots look different from the others because there are two peaks in each plot. The first peak (that is, the peak at lower mass/the right peak) is where a D^+ particle has decayed to either $K_s\pi$ or K_sK. The second/higher mass peak is where a D_s^+ particle has decayed to either $K_s\pi$ or K_sK. The D_s^+ decays are Cabibbo supressed. One of the more interesting problems of the summer was reflection in the $K_s\pi$ data. We added two functions to the fit for $K_s\pi$ to account for reflections from K_sK. These reflections occur when the second kaon in K_sK data is misidentified as a pion. To create these functions we used K_sK Monte Carlo that had been misidentified as $K_s\pi$. The reflection from $D^+ \rightarrow K_sK$ is the blue function in fig. 17 and the reflection from $D_s \rightarrow K_sK$ is the red function.

4 Uncertainties

The uncertainties in our branching ratios can be broken down into two main types: statistical and systematic. There are many types of systematic uncertainties. Each uncertainty described below was added in quadrature to get a total relative systematic uncertainty. This value is factored into the upper-limit calculation for channels in which no signal was observed or it is quoted with the branching ratio in the case the a signal is observed.

4.1 Statistical

The stastical uncertainty was a fairly simple calculation in which the uncertainty in the yield was divided by the yield for both normalization data and Monte Carlo and the signal Monte Carlo. All three statistical uncertainties were added in quadrature to get an overall statistical uncertainty. These stastical uncertainties were then factored into the total relative systematic uncertainty. The stastical uncertainty on the signal data is reported with the branching ratio.

4.2 Systematic

We had many measures of systematic uncertainty. These include how the data was fit, whether the Monte Carlo included resonance, how the branching ratios changed as the cuts were varied, and the inherent tracking uncertain-

ties of the experiment.

To determine the uncertainty due to the fitting function for the Monte Carlo, both the normalization and signal Monte Carlo were fit two ways. The first was a single Gaussian function with a quadratic background; the second was a double Gaussian function with a quadratic background. We took the percent difference between the ratio of the yields from the signal and normalization Monte Carlo fit with a single Gaussian function and the ratio of the yields from the signal and normalization Mont Carlo fit with a double Gaussian function. To determine the uncertainty due to the fitting function for the normalization data, we fit it with a single Gaussian function and a double Gaussian function (both with quadratic backgrounds). We took the percent difference in yield between the two as our measure of uncertainty. The fit uncertainty from the Monte Carlo was added in quadrature with the fit uncertainty from the normalization data to determine an overall fit uncertainty.

Resonance occurs when a D particle (in our case) decays to intermediate particles and then those particles decay to the final products. $K_s5\pi$, for example, can decay as follows: $D^+ \rightarrow K_s a_1^+$ and $a_1^+ \rightarrow \rho(1450)\pi^+$ and $\rho(1450) \rightarrow \pi^+\pi^-\pi^+\pi^-$. The uncertainty due to resonance was calculated through the use of resonant and non-resonant Monte Carlo. We fit the resonant and non-resonant Monte Carlo identically (using the same function and same cuts) and took the percent difference in the yields as our measure of uncertainty.

Another measure of systematic uncertainty was the stability of the branching ratios as the cuts were varied. Branching ratios depend on both data and Monte Carlo, which is simulation of the data. If the Monte Carlo accurately simulates the data, the branching ratio should remain constant, even if the cuts are changed. We use this uncertainty because it is impossible to perfectly model the data. For the three channels in which no signal was seen ($K_s6\pi$, $K_s5\pi$, and $3K_s\pi$), we recorded the corrected yield (data yield divided by Monte Carlo yield) of the normalization mode while varying each cut individually. We then took the standard deviation of the corrected yields as our uncertainty. For the channel in which we saw signal ($K_s\pi$), we used a similar process, except that we used the branching ratio instead of the corrected yield.

The last systematic uncertainty was due to the tracking efficiencies inherent in the experiment. The uncertainty on charged tracks is .2% and the uncertainty on K_s tracks is 7.1 %.

	Statistical	Systematic (fit)	Systematic (resonance)	Cut Stability	Tracking Uncertainty
$K_s6\pi/K_s4\pi$	0.048	0.131	0.231	0.001	0.004
$K_s5\pi/K_s3\pi$	0.014	0.082	0.074	0.001	0.004
$3K_s\pi/K_s3\pi$	0.020	0.051	0.040	0.001	0.137
$K_s\pi/K_sK$	0.063	0.445	0.000	0.013	0.000

	Total Relative Systematic Uncertainty
$K_s6\pi/K_s4\pi$	0.270
$K_s5\pi/K_s3\pi$	0.112
$3K_s\pi/K_s3\pi$	0.153
$K_s\pi/K_sK$	0.450

5 Conclusion

5.1 Branching Ratios and Upper Limits

For the channels in which no signal was seen, we cannot calculate a definitive branching ratio. Instead, we calculate an 95% confidence level upper limit on the branching ratio. To do so, we integrated the branching ratio likelihood function

$$p(B) \propto \frac{1}{\sqrt{\frac{B^2}{\sigma_B^2}+\frac{1}{\sigma_\epsilon^2}}} \exp\left[\frac{-(B-\hat{B})^2}{2(B^2\sigma_\epsilon^2+\sigma_B^2)}\right]\left\{\mathrm{erf}\left[\frac{B\hat{B}\sigma_\epsilon^2+\sigma_B^2}{\sqrt{2}\sigma_\epsilon\sigma_B\sqrt{B^2\sigma_\epsilon^2+\sigma_B^2}}\right]-\mathrm{erf}\left[\frac{(\hat{S}-1)\sigma_B^2-B\sigma_\epsilon^2(B-\hat{B}\hat{S})}{\sqrt{2}\hat{S}\sigma_\epsilon\sigma_B\sqrt{B^2\sigma_\epsilon^2+\sigma_B^2}}\right]\right\}$$

from 0 to our upper limit L. That is, $0.95 = \int_0^L p(B)dB$. The results are given in the table below.

	Upper Limit Branching Ratio
$K_s6\pi/K_s4\pi$	0.0135
$K_s5\pi/K_s3\pi$	0.0034
$3K_s\pi/K_s3\pi$	0.0035

Because we observed a signal in $D_s \rightarrow K_spi$, we quote a conventional branching ratio.

	Branching Ratio
$K_s\pi/K_sK$	0.223±.100±.04

5.2 Final Thoughts

The results I found this summer will eventually be published, so I intend to continue working with Profs. Cumalat and Stenson after the REU program is finished. We still have some work to do on the all the channels. I would like to say tank you to Profs. Cumalat and Stenson for making this summer such a positive experience, for giving me the opportunity to tour Fermilab and give a talk to the FOCUS collaboration, and for being extremely patient with a clueless undergraduate physics student.

I would also like thank everyone involved with the REU program for offering research opportunities to undergraduates. I consider my time at the University of Colorado an extremely valuable. Thank you for letting me be involved in "real" physics.

References

[1] Eric W. Vaadering, Ph.D. thesis, University of Colorado at Boulder, 2000.

[2] FOCUS Collaboration, http://www-focus.fnal.gov, August 9, 2006.

[3] J.M. Link et.al. [FOCUS Collaboration], "A Study of $D^0 \rightarrow K^0_s K^0_s X$ decay channels," Phys. Lett. B607, 59 (2005)

[4] Kevin Stenson, "A more exact solution for incorporating multiplicative systematic uncertainties in branching ratio limits," University of Colorado at Boulder.